APPENDIXES

Appendix A

List of deposited films

APPENDIX A – List of deposited films

The following tables show the films and multilayer structures that have been deposited in the Departament de Física Aplicada i Òptica. Each table lists chronologically the samples, whose coding includes this information:

material ; date ; sample number	(generic)
WDLC 030121-2	(example)

The first two tables include DLC samples prepared in the PECVD reactor (section 3.1), whereas the rest of depositions were carried out in the sputtering reactor (section 3.2). All the depositions were performed up to 50ºC temperature. The technological parameters concerning each deposition are registered in these tables.

DLC films deposited by pulsed-DC PECVD

NAME	Voltage (V)	Intensity (A)	Power (W)	Frequency (kHz)	Bias voltage (V)	Thickness (nm)	Deposition rate (nm/min)
DLC 020621-1	232.2	0.43	100	200	-800	230	23
DLC 020621-2	91.0	0.25	23	200	-400	135	4.5
DLC 020621-3	333.8	0.08	26	100	-800	260	8.7
DLC 020625-1	430	0.09	42	100	-1000	300	10
DLC 020625-2	298	0.53	158	200	-1000	370	52.9
DLC 020626-1	372	0.31	115	150	-900	475	47.5
DLC 020627-1	368	0.31	115	150	-900	400	40
DLC 020627-2	522.2	0.12	62	100	-1200	700	35
DLC 020627-3	518	0.40	210	150	-1200	535	53.5
DLC 020627-4	424	0.34	145	150	-1000	750	50
DLC 020627-5	531	0.22	121	125	-1100	350	35
DLC 020628-1	531	0.23	122	125	-1100	600	60
DLC 020701-1	422	0.34	145	150	-1000	980	65.3
DLC 020722-1	518	0.40	210	150	-1200	620	62
DLC 020722-2	562	0.24	135	125	-1200	600	60
DLC 020722-3	603	0.14	84	100	-1400	520	52
DLC 020722-4	451	0.19	89	125	-1000	480	48
DLC 020722-5	429	0.34	149	150	-1000	550	55
DLC 020726-2	284	0.14	40	125	-665	365	24.3
DLC 020726-3	227.6	0.21	50	150	-600	315	21
DLC 031211-1	405	0.10	43	100	-1000	275	13.7
DLC 031211-2	320	0.08	27	100	-800	225	7.5
DLC 040126-1	245	0.06	16	100	-600	150	3.3
DLC 040126-2	500	0.12	64	100	-1200	245	24.5
DLC 040126-3	590	0.15	90	100	-1400	350	35
DLC 040303-1	410	0.10	44	100	-1000	680	11.3
DLC 040304-1	407	0.10	44	100	-1000	160	10.7
DLC 040305-1				100	-1000	1400	14
DLC 040309-1	330	0.54	180	200	-1000	530	53
DLC 040310-1	413	0.34	142	150	-1000	420	42
DLC 040310-2	450	0.20	92	125	-1000	380	38

DLC films deposited by RF PECVD

NAME	Power (W)	Modulation frequency (kHz)	Duty cycle (%)	Bias voltage (V)	Thickness (nm)	Deposition rate (nm/min)
DLC 020604-2	210	20	20	-800	450	15
DLC 020604-3	52	20	20	-400	250	6.6
DLC 020607-1	115	20	20	-600	400	7.3
DLC 020603-1		-	-	-600	550	36.6
DLC 020603-2		-	-	-800	450	45
DLC 020603-3		-	-	-600	350	35
DLC 020603-4		-	-	-400	500	25
DLC 020603-5		-	-	-200	300	12
DLC 020604-1		-	-	-200	500	10

Me-DLC (Me = Mo, Nb, Ti, W) films deposited by pulsed-DC reactive magnetron sputtering

NAME	Pressure (Pa)	Relative CH_4 flow (%)	RF power (W)	RF bias (V)	Pulsed-DC power (W)	Voltage (V)	Intensity (A)	Pulsed bias (V)	Thickness (nm)	Deposition rate (nm/min)
DLC 020429-1	5	100	49.5	-500	0	-	-	-	600	20
DLC 020502-1	0.2	100	49.5	-520	0	-	-	-	60	2
DLC 020503-1	5	100	19.5	-300	0	-	-	-	425	9.4
DLC 020503-2	10	100	54.5	-500	0	-	-	-	550	36.7
DLC 020503-3	10	100	22	-300	0	-	-	-	610	20.3
DLC 020508-1	10	100	12.5	-200	0	-	-	-	550	11
DLC 020508-2	5	100	10.5	-200	0	-	-	-	700	5.8
DLC 020510-1	10	100	5	-100	0	-	-	-	520	3.7
DLC 020510-2	5	100	4.5	-100	0	-	-	-	775	1.9
DLC 020522-1	10	50	-	-200	0	-	-	-	550	6.11
DLC 020523-1	10	75	8.5	-200	0	-	-	-	550	7.9
DLC 020524-1	10	25	8.5	-200	0	-	-	-	900	6
MoDLC 020626-4	10	25	7	-230	100	270	0.37		260	8.7
Mo 020626-5	10	0	11	-240	100	165	0.6	-	15	0.75
MoDLC 020626-6	10	1	11	-200	100	192	0.52	-648	20	1
MoDLC 020627-1	10	3	8.5	-120	100	220	0.44	-	25	1.25
MoDLC 020627-2	5	3	7.5	-228	100	220	0.45	-616	100	5
Mo 020628-1	5	0	7.5	-200	100	190	0.53	-520	80	4

NAME	Pressure (Pa)	Relative CH_4 flow (%)	RF power (W)	RF bias (V)	Pulsed-DC power (W)	Voltage (V)	Intensity (A)	Pulsed bias (V)	Thickness (nm)	Deposition rate (nm/min)
MoDLC 020628-2	5	25	6.5	-220	100	230	0.43	-	110	5.5
MoDLC 020701-1	5	25	7	-240	100	245	0.41	-640	550	5.5
DLC 020701-2	5	25	9	-222	0	-	-	-	330	3.3
MoDLC 020702-1	7.5	14	-	-238	100	267	0.37	-720	100	5
TiDLC 020704-1	5	25	-	-	100	-	-	-	490	6.12
Ti 020704-2	5	0	8	-200	100	-	-	-	15	1
TiDLC 020705-1	5	3	-	-	100	-	-	-	145	2.4
Ti 020705-2	10	0	10	-230	100	-	-	-	350	8.75
TiDLC 020705-3	10	3	-	-	100	-	-	-	20	0.45
TiDLC 020708-1	7.5	14	7	-220	100	-	-	-	130	4.3
TiDLC 020708-2	10	3	6	-195	100	-	-	-	15	0.3
TiDLC 020710-1	10	25	6.5	-225	100	-	-	-	305	7.6
WDLC 020716-1	5	1	6	-210	100	-	-	-	219	5.5
WDLC 020716-2	5	3	7	-215	100	-	-	-	295	9.8
NbDLC 020716-3	5	1	9.5	-200	100	-	-	-	120	3
NbDLC 020716-4	5	3	9	-205	100	-	-	-	122	4.06
Nb 030116-1	5	0	7	-200	100	220	0.45	-552	150	2.5
NbDLC 030117-1	5	4	7	-210	100	390	0.25	-960	80	3.2
NbDLC 030117-2	5	6	7	-210	100	390	0.25	-968	210	3.5
W 030120-1	5	0	7	-210	100	218	0.46	-600	380	7.6

NAME	Pressure (Pa)	Relative CH_4 flow (%)	RF power (W)	RF bias (V)	Pulsed-DC power (W)	Voltage (V)	Intensity (A)	Pulsed bias (V)	Thickness (nm)	Deposition rate (nm/min)
WDLC 030120-2	5	6	7	-215	100	300	0.33	-792	245	8.17
WDLC 030121-1	5	2	7	-220	100	260	0.38	-712	180	7.2
WDLC 030121-2	5	3	7	-220	100	275	0.36	-736	235	9.4
WDLC 030122-1	5	25	7	-220	100	232	0.43	-600	185	6.2
TiDLC 030127-1	5	2	7	-245	100	230	0.43	-624	62.5	1.04
TiDLC 030128-1	5	6	7	-230	100	274.5	0.36	-736	150	2.7
MoDLC 030129-1	5	6	7	-230	100	233	0.43	-648	160	4
MoDLC 030129-2	5	10	7	-235	100	280	0.35	-760	160	4
Nb 030506-1	5	0	10.5	-195	100	245	0.41	-624	145	2.4
NbDLC 030506-2	5	1	10.5	-195	100	292	0.34	-712	75	1.7
NbDLC 030506-3	5	3	10.5	-205	100	417	0.24	-1000	35	1.17
NbDLC 030507-1	5	10	9.5	-205	100	355	0.28	-872	190	4.22
NbDLC 030507-2	5	25	9.5	-190	100	-	-	-	280	7.6
NbDLC 030507-3	5	3	9.5	-200	100	400	0.25	-968	50	
Ti 030604-1	5	0	6.5	-215	100	188	0.53	-528	90	1.5
TiDLC 030610-1	5	1	6	-200	100	215	0.46	-584	62.5	1.04
TiDLC 030610-2	5	3	6	-210	100	230	0.43	-624	130	2.2
TiDLC 030611-1	5	3	6	-205	100	228	0.44	-650	145	2.4
TiDLC 030612-1	5	10	6.5	-205	100	250	0.40	-680	170	2.8
W 030616-1	5	0	5.5	-205	100	260	0.38	-	250	8.3

NAME	Pressure (Pa)	Relative CH_4 flow (%)	RF power (W)	RF bias (V)	Pulsed-DC power (W)	Voltage (V)	Intensity (A)	Pulsed bias (V)	Thickness (nm)	Deposition rate (nm/min)
WDLC 030617-1	5	1	5.5	-205	100	280	0.35	-	180	6
WDLC 030617-2	5	3	5.5	-205	100	300	0.30	-	270	9
WDLC 030618-1	5	10	5.5	-205	100	340	0.29	-872	250	8.3
W 040416-1	5	0	6.5	-205	100	185	0.53	-540	200	6.7

Me and DLC films deposited by RF magnetron sputtering

NAME	Pressure (Pa)	Ar flux (sccm)	RF power (W)	RF bias (V)	Modulation frequency (Hz)	Duty cycle (%)	Bias voltage (V)	Thickness (nm)	Deposition rate (nm/min)
W 010502-1	0.16	4	50	-125	-	-	0	125	12.5
W 010502-2	0.16	4	50	-135	-	-	1.65	125	12.5
W 010504-1	0.16	4	50	-130	-	-	2	380	12.7
DLC 010517-1	0.21	5	300	-600	-	-	16.2	300	15
DLC 010518-1	0.2	5	100	-295	-	-	9.2	145	3.22
DLC 010518-2	0.2	5	200	-450	-	-	14.5	195	9.75
DLC 010606-1	0.2	5	300/10	-235	125	50	7	90	6
DLC 010607-1	0.21	5	300/10	-330	50	50	8	90	6
DLC 010607-2	0.21	5	300/10	-240	30	30	4/8	60	4
DLC 010705-1	0.28	7	300/10	-230	30	30	7	150	3.75

Me/a-C (Me = Mo, W) multilayer structures deposited by RF magnetron sputtering

NAME	Pressure (Pa)	Ar flux (sccm)	RF power to Me (W)	Deposition time Me (s)	RF power to graphite (W)	Deposition time C (s)	Bias voltage (V)	Number of bilayers	Thickness (nm)
W/a-C 010523-1	0.2	5	50	20	100	180	11.3	15	220
W/a-C 010608-1	0.21	5	50	20	300/10	120	6.5	15	180
W/a-C 010608-2	0.21	5	50	20	300/10	180	6	15	230
W/a-C 010608-3	0.21	5	50	20	300/10	60	6.5	15	120
W/a-C 020604-1	0.2	5	50	10	300/10	30		30	35
W/a-C 020606-1	0.2	5	50	10	300/10	30	-40	30	60
W/a-C 020607-1	2	50	50	10	300/10	30	-40	30	-
W/a-C 020607-2	2	50	50	10	300/10	30	-300	30	-
W/a-C 020607-3	0.2	50	50	10	300/10	30	-300	30	600
W/a-C 020607-4	1.1	40	50	10	300/10	30	-170	30	70
W/a-C 020711-1	0.2	30	50	20	300/10	30	-40	30	85
W/a-C 020711-2	0.8	40	50	20	300/10	30	-40	30	96
W/a-C 020712-2	2	50	50	20	300/10	30	-40	30	70
W/a-C 020712-3	2	50	50	20	300/10	30	-300	30	37
W/a-C 020712-4	0.2	30	50	20	300/10	30	-300	30	30
W/a-C 020712-5	1.1	40	50	20	300/10	30	-170	30	52
W/a-C 020712-6	0.2	30	50	20	300/10	30	-40	30	79
Mo/a-C 020712-7	0.2	30	50	20	300/10	30	-40	30	46

NAME	Pressure (Pa)	Ar flux (sccm)	RF power to Me (W)	Deposition time Me (s)	RF power to graphite (W)	Deposition time C (s)	Bias voltage (V)	Number of bilayers	Thickness (nm)
Mo/a-C 020715-2	2	50	50	20	300/10	30	-40	30	47
Mo/a-C 020715-3	2	50	50	20	300/10	30	-300	30	109
Mo/a-C 020715-4	0.2	30	50	20	300/10	30	-300	30	31
Mo/a-C 020715-5	1.1	40	50	20	300/10	30	-170	30	105

Appendix B

Spontaneous formation of nanometric multilayers in Ti-DLC films

Appendix B – Spontaneous formation of nanometric multilayers in Ti-DLC films

Chapter 8 deals with the nanostructure of metal containing DLC films. Among the different metals added to DLC amorphous matrix, we can remark the special structure acquired by Ti-DLC. Its growth was characterized by the alternated stacking of C- and Ti- rich layers, which provides a multilayer pattern. As explained below, this spontaneous arrangement in separated layers can be interpreted as the tendency to phase segregation by a mechanism of up-hill diffusion [Corbella C., in press]. This is equivalent to consider that diffusion coefficient acquire negative values in certain regions of phase diagrams.

Spontaneous nanostructuring in Me-DLC thin films is an interesting possibility, since in most cases equilibrium phase diagrams present wide ranges of metal content and temperature in which homogeneous phases are thermodynamically unstable. Annealing of films grown inside such a miscibility gap can enhance up-hill diffusion, and hence facilitate segregation [Kim H., 2002], which has been associated to large changes in properties such as hardness [Knotek O., 1989]. But already during film growth, the deposited atoms dispose of an excess of energy to diffuse, which is subject to being experimentally controlled. Furthermore the intrinsic anisotropy of the growth process, together with its non-equilibrium character, may induce nontrivial morphological effects at segregation scales. In this appendix, we have explored this possibility for the Ti-C system, whose equilibrium miscibility gap spans from 0% to 50% at. Ti for temperatures below 3049 K.

B.1. Bases of the model

We propose that the layering occurs as a non-equilibrium process, through the mechanism of *spinodal decomposition* [Daruka I., 2005] in which atomic interactions, favouring atoms of the same species, overcome the tendency to maximize entropy, producing up-hill diffusion. Then, an initially thermodynamically unstable concentration of Ti-C develops spatial modulations, segregating into Ti- and C- rich amorphous phases. Contrary to nucleation, spinodal decomposition induces segregation through compositional modulations of a well defined wavelength [Cahn J.W., 1968].

This mechanism can produce noticeable changes in composition within the time scales of the experiment because, during film growth, the deposition energy of the atoms can dramatically enhance diffusivity near the surface of the film by many orders of magnitude [Dahan I., 2000] [Swart H.C., 2003] [Arvieu C., 2004]. The diffusivity takes then appreciable values in a narrow region near the growing interface, related to the penetration depth of the deposited atoms. The bands observed at the Ti-DLC films with 60%, 25%, and 5% at. Ti would thus be due to spinodal decomposition in this external layer.

The model used to study spinodal decomposition consists in a Cahn-Hilliard equation for bulk phase separation, supplemented with a surface-potential term at the substrate. From the concentration of carbon we define a new variable:

$$u = (2c - c_\beta - c_\alpha)/(c_\beta - c_\alpha) \tag{B.1}$$

where c_α and c_β are the carbon concentrations in the Ti-rich and C-rich metastable amorphous states. The evolution of this variable obeys a conservation equation:

$$\partial_t u = -\vec{\nabla}\cdot\vec{j} \tag{B.2}$$

with the flux, $\vec{j}$, being related to a field, ϕ, and the chemical potential, μ, by means of:

$$\vec{j} = D(1-\phi^2)\vec{\nabla}\mu \tag{B.3}$$

where D is the diffusion coefficient. The flux of carbon atoms takes negligible values except in a region of width l_D near the surface, where the atoms have enough energy to diffuse. This is enforced by defining a field:

$$\phi = \tanh[(z - v_{fg}t)/l_D] \tag{B.4}$$

which separates the film (ϕ=-1), where material has been deposited, from the plasma (ϕ=1), with a diffuse interface of width ~l_D in the z-direction. The film surface thus grows with velocity v_{fg}, which depends on the deposition rate.

The chemical potential of the binary system has minima corresponding to the two metastable states (c=c_α and c=c_β), and is defined as:

$$\mu = u - u^3 + \kappa^2 \nabla^2 u + V(z) \tag{B.5}$$

It includes a term accounting for the interfacial energy, κ, which is the gradient energy coefficient, and a potential, V, that incorporates the larger affinity of the substrate for one of the components:

$$V(z) = \begin{cases} h_1, & z < z_0 \\ h_1 z_0^2 / z^2, & z > z_0 \end{cases} \tag{B.6}$$

These equations have been solved with an explicit scheme and assuming non-flux boundary conditions. We consider that the deposited concentration fluctuates around an average value:

$$u = u_0 + \xi(\vec{r}) \tag{B.7}$$

with

$$\langle \xi(\vec{r}'), \xi(\vec{r}) \rangle = \sigma^2 \delta(\vec{r}' - \vec{r}) \tag{B.8}$$

B.2. Simulations

We have tested the scenario described above by numerical simulations of a modified version of the Cahn-Hilliard model of phase separation [Cahn J.W., 1958]. The basic ingredients of this model are the species diffusivity, and the bulk and interfacial free energies. The wavelength of the developing segregation pattern, λ_{sp}, is then given solely by the ratio between the curvature of the free energy curve at the given initial concentration, and the interfacial gradient coefficient. Together with the diffusivity, these parameters also provide the time scale in which the bands appear. The model has been completed with a length scale, l_D, corresponding to the width of the superficial layer on which diffusion is enhanced, and an interaction term [Puri S., 2002] taking into account the affinity of the Ti atoms to the Si substrate.

The equations from section B.1 have been simulated in a box $L_z \times L_x = 40 \times 80$, for various values of u_0 and v_{fg}. For the other non-dimensional parameters we take κ^2=0.4, l_D=2, h_1=-1, z_0=4, D=0.5, and σ=0.2

Results show that the interaction with the substrate, which acts during the early stages of film growth, together with the inherent periodicity of the spinodal decomposition process, is enough for coherent formation of the successive layers.

Simulation patterns obtained for increasing values of C concentration are shown in figures B.1(a), B.1(b) and B.1(c) in a case with large growth velocity v_{fg}. The initial segregation induced by the presence of the substrate is more effective in the middle of the miscibility gap, but is only able to form a few layers during a small transient, since the time during which diffusion is enabled at a given point ($t \sim l_D / v_{fg}$) is shorter than the time scale for segregation. By reducing the growth speed, almost perfect bands are produced (figure B.1(d)).

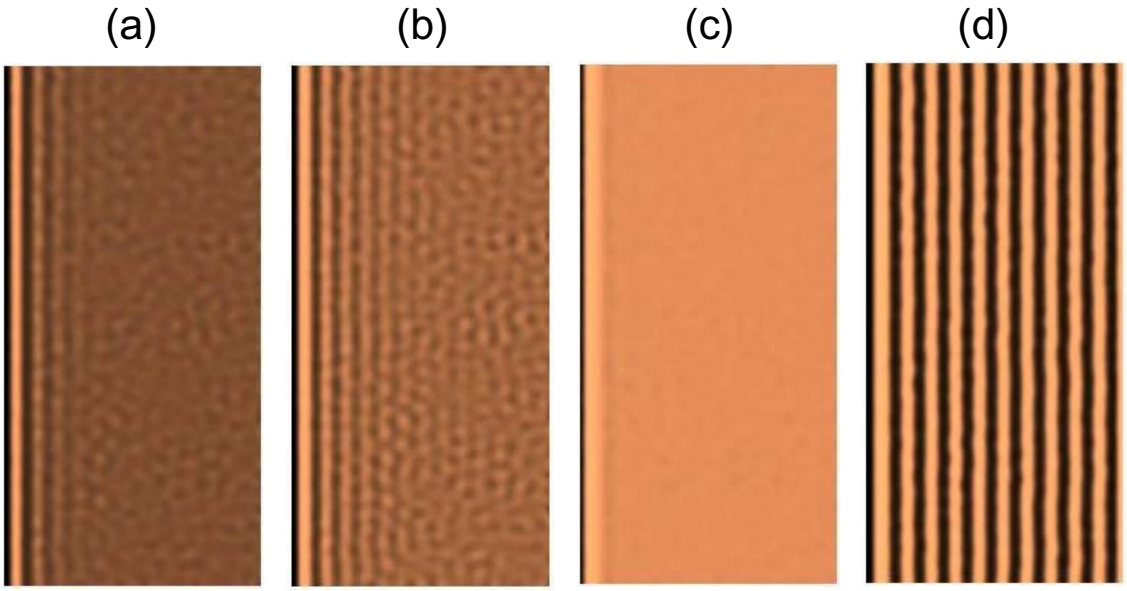

Figure B.1: Simulation patterns of Ti-C multilayers generated with the Cahn-Hilliard model for phase separation. The effects of changing the concentration and growth velocity on film banding are shown (with dark and light bands corresponding to Ti- and C-rich regions, respectively). The concentration is (a) u_0=-0.2, (b) u_0=0, (c) u_0=0.4, with a surface growth velocity v_{fg}=0.6, and (d) u_0=0, with a slower growth velocity v_{fg}=0.3.

Appendix C

Physics of glow discharges

Appendix C – Physics of glow discharges

This appendix continues the introductory part of plasmas from chapter 1, and its aim is to introduce the basic concepts in physics of low-pressure plasmas. First of all, a brief section defines the most relevant plasma parameters: plasma density, ionisation degree and plasma temperature. Such introduction is followed by a description of physical processes in glow discharges. In this second section, the abundant use of mathematical expressions is to provide a rigorous review to the most important plasma concepts. Beginning with some fundamental expressions in Electromagnetism, which are inferred from Maxwell's equations, the discussion takes place in the background of phase space and the conservation equations of the distribution functions. After that, the main plasma parameters are defined and, finally, the last section deals with transport phenomena in plasma dynamics.

More specific aspects of glow discharges like motion of charge carriers within electric and magnetic fields, and collision theory, demand a solid knowledge of quantum mechanics and electrodynamics. These aspects have not been considered, although they constitute fields in plasma research that have been extensively studied.

C.1. Definition of plasma parameters

The following variables are considered the main plasma parameters, i.e. their values characterise more or less accurately the plasma state:

(i) *Plasma density*:

The abundance of species is quantified by their corresponding densities: density of electrons, n_e, positive ions, n_i^+, negative ions, n_i^-, and neutrals, n_g. According to these parameters, we can define an electropositive gas:

$$n_e \approx n_i^+ \tag{C.1}$$

as well as an electronegative gas:

$$n_e + n_i^- \approx n_i^+ \tag{C.2}$$

(ii) *Ionisation degree*:

The ionisation degree, X_{iz}, measures the ion population to all species rate:

$$X_{iz} = \frac{n_i}{n_g + n_i} \tag{C.3}$$

Plasmas are considered as fully ionised when it is of the order of 1, whereas weakly ionised gases exhibit degrees lower than 10^{-3}.

(iii) *Plasma temperature*:

This constitutes a measurement of the mean kinetic energy of each species. Thus, temperatures are assigned to electrons, T_e, ions, T_i, and neutrals, T_g. Generally, they are not identical, unless at thermodynamic equilibrium conditions, where:

$$T_e \approx T_i \approx T_g \tag{C.4}$$

This is the condition of thermal plasma. Oppositely, cold plasma is out of equilibrium and the corresponding temperatures show the following relationship:

$$T_e >> T_i \geq T_g \tag{C.5}$$

C.2. Basic equations in glow discharges

· Electromagnetism

In this section, the basic equations of plasmas have been obtained. The first step consists of considering the Maxwell's equations, which are the fundamental expressions in Electromagnetism. They establish the main relationships between electric field, *E*, and magnetic field, *B*, taking into account their corresponding sources and the nature of the medium. They can be written either in differential or integral form, but the former is more useful for the discussion below. The following are the Maxwell's equations in vacuum [Liebermann M.A., 2005]:

$$\nabla \cdot \vec{E} = \frac{\rho}{\varepsilon_0} \tag{C.6}$$

$$\nabla \cdot \vec{B} = 0 \tag{C.7}$$

$$\nabla \times \vec{E} = -\frac{\partial \vec{B}}{\partial t} \tag{C.8}$$

$$\nabla \times \vec{B} = \mu_0 \left(\vec{j} + \varepsilon_0 \frac{\partial \vec{E}}{\partial t} \right) \tag{C.9}$$

Here, ρ is the electric charge density, j is the electric current, ε_0 is the vacuum electric permittivity, and μ_0 is the vacuum permeability. Equations C.6 and C.7 are called Gauss' law for electricity and magnetism, respectively, and relate the flux of electric and magnetic fields to charges. Equation C.8 is the Faraday's law of induction, and equation C.9 is the Ampere's law, which impose restrictions for both $\vec{E}$ and $\vec{B}$. Since plasmas often show a negligible time variation of $\vec{B}$, the Faraday's law indicates the existence of a scalar potential, ϕ, that defines $\vec{E}$:

$$\vec{E} = -\nabla \phi \tag{C.10}$$

The Poisson's equation is used to infer electric potential from charge distribution, and is obtained if equation C.10 is substituted in the Gauss' law for $\vec{E}$:

$$\nabla^2 \phi = -\frac{\rho}{\varepsilon_0} \tag{C.11}$$

The Lorentz's force, F_L, is basic to determine the electrodynamics of charged species influenced by an electromagnetic field:

$$\vec{F}_L = q\left(\vec{E} + \vec{v} \times \vec{B}\right) \tag{C.12}$$

where q is the charge and $\vec{v}$ is the velocity of the specie. Another electromagnetic equation of relevance is the continuity equation, which provides a close relationship between the sources of electromagnetic fields:

$$\frac{\partial \rho}{\partial t} + \nabla \cdot \vec{j} = 0 \tag{C.13}$$

which means that charge is locally conserved.

· Conservation equations

The microscopic description of a plasma, and in general of a thermodynamic system, is given by the particles distribution function, f, in the phase space. This consists on a 6-D space, where every particle has assigned three dimensions for its position, $\vec{r}$, and other three ones for its velocity (figure C.1).

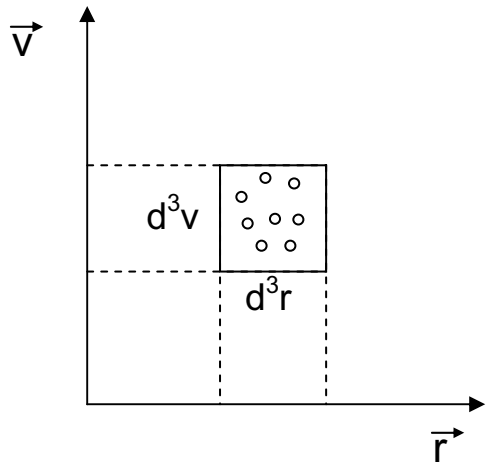

Figure C.1: Representation of particles confined in an elemental volume $d^3r \cdot d^3v$ of the phase space.

The physical interpretation of $f(\vec{r},\vec{v},t) \cdot d^3r \cdot d^3v$ is the number of particles inside a 6-D phase space volume $d^3r \cdot d^3v$ at figurative point $(\vec{r},\vec{v})$ at time t. This distribution function satisfies the Boltzmann equation:

$$\frac{\partial f}{\partial t} + \vec{v} \cdot \nabla_r f + \frac{\vec{F}}{m} \cdot \nabla_v f = \frac{\partial f}{\partial t}\Big|_C \tag{C.14}$$

where m is the particle mass and right side of the equation represents a collisional term. By means of this function we can calculate macroscopic magnitudes, as the particle density, n, and the particle flux, Γ:

$$n(\vec{r},t) = \int f(\vec{r},\vec{v},t)\cdot d^3v \tag{C.15}$$

$$\Gamma(\vec{r},t) = n\cdot\vec{u} = \int \vec{v}\cdot f(\vec{r},\vec{v},t)\cdot d^3v \tag{C.16}$$

where $\vec{u}$ is the average velocity. The equations that describe the temporal evolution of these macroscopic quantities are the macroscopic conservation equations: particle, momentum and energy conservation. Particle conservation is expressed by a continuity equation, which is obtained by integrating all the terms of Boltzmann equation over velocity space:

$$\frac{\partial n}{\partial t} + \nabla\cdot(n\vec{u}) = G - L \tag{C.17}$$

where G and L represent the source and sink terms for particles, respectively. Momentum (equation C.18) and energy (equation C.19) conservation equations are the results of integrating Boltzmann equation after multiplying it by $\vec{v}$ and $m\vec{v}/2$, respectively:

$$mn\left[\frac{\partial\vec{u}}{\partial t} + (\vec{u}\cdot\nabla)\vec{u}\right] = qn(\vec{E} + \vec{u}\times\vec{B}) - \nabla\cdot\Pi + f\big|_C \tag{C.18}$$

$$\frac{\partial}{\partial t}\left(\frac{3}{2}p\right) + \nabla\cdot\frac{3}{2}(p\vec{u}) + p\nabla\cdot\vec{u} + \nabla\cdot\vec{q} = \frac{\partial}{\partial t}\left(\frac{3}{2}p\right)\Big|_C \tag{C.19}$$

where p is the gas pressure and Π is the pressure tensor. It is demonstrable that in thermodynamic equilibrium or kinetic equilibrium for each species separately, and without temporal variations, spatial gradients and acceleration, the collisional term in equation C.14 is zero and the Boltzmann equation is satisfied by the Maxwell-Boltzmann (MB) distribution function for the velocities:

$$f(v) = n\left(\frac{m}{2\pi kT}\right)^{3/2}\exp\left[-\frac{mv^2}{2kT}\right] \tag{C.20}$$

where k is the Boltzmann constant and T is the absolute temperature. The MB distribution function is used to calculate averaged quantities such as average velocity and average energy.

· Plasma dynamics

By integrating the electron force balance obtained from momentum conservation expression (equation C.18) in the absence of electron drifts, we obtain the Poisson-Boltzmann relation for electrons:

$$n_e(\vec{r}) = n_0 \exp\left(\frac{e\phi(\vec{r})}{kT_e}\right) \tag{C.21}$$

It permits to define the electron Debye length, λ_{De}, which is the characteristic length scale in a plasma. Its physical meaning is explained by considering the following situation. If a negatively charged sheet is immersed into a plasma having equilibrium densities n_e=n_i=n_0, and assuming immobile ions, the 1-D Poisson's equation results as follows:

$$\frac{d^2\phi}{dx^2} = -\frac{e}{\varepsilon_0}(n_i - n_e) \tag{C.22}$$

If we substitute n_e by its expression set in equation C.21, and imposing n_e=0 at infinity, we obtain the following solution to equation C.22:

$$\phi(x) = \phi_0 \exp(-|x|/\lambda_{De}) \tag{C.23}$$

where the Debye length is defined [Woods L.C., 2004]:

$$\lambda_{De} = \left(\frac{\varepsilon_0 kT_e}{en_0}\right)^{1/2} \tag{C.24}$$

As shown in equation C.23, λ_{De} is the distance scale in plasmas over which potential gradients vanish. For low-pressure plasmas, λ_{De} ~ 0.1 mm. T_e, n_e, and λ_{De} are fundamental parameters in plasmas. Along with plasma potential, their values are of great utility in the discussion of glow discharge properties in chapter 5. Some techniques to measure them are mentioned in chapter 3.

The parameter λ_{De} restricts sheath dimensions and fulfils this relation:

$$\lambda_{De} = v_{Te}/\omega_{pe} \tag{C.25}$$

where v_{Te} is the electron thermal velocity and ω_{pe} is the electron plasma frequency:

$$\omega_{pe} = \left(\frac{e^2 n_0}{\varepsilon_0 m}\right) \tag{C.26}$$

being m the electron mass. It can be considered the fundamental characteristic frequency of the plasma, ω_p, since vibrational amplitude of ions, ω_{pi}, is neglected as a consequence of infinite ion mass assumption:

$$\omega_p = (\omega_{pe}^2 + \omega_{pi}^2)^{1/2} \approx \omega_{pe} \tag{C.27}$$

This frequency has a clear physical meaning. The electron cloud in a plasma oscillate with respect to the ion cloud at this natural frequency, when both clouds are displaced as

response of an external perturbation (figure C.2). This is a mechanism to keep the electric quasineutrality in plasmas.

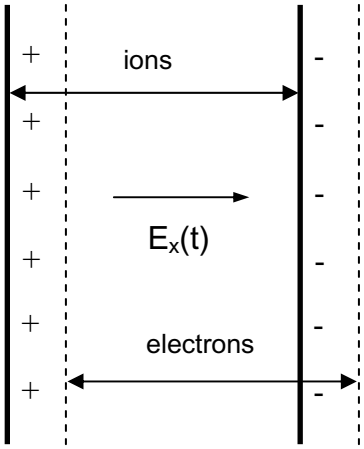

Figure C.2: The action of an electric field $E_x(t)$ due to the displacement of electron cloud with respect to the ion cloud yields plasma oscillations.

Transport of ions and electrons through a plasma is described by a law of free diffusion. By considering the momentum conservation equation (C.18), the particle flux, Γ, can be expressed in terms of a few parameters:

$$\Gamma = \pm \mu n \vec{E} - D \nabla n \tag{C.28}$$

Here, μ is the mobility of the species, and D is the diffusion coefficient. In the absence of an electric field, the diffusion equation is obtained:

$$\Gamma = -D \nabla n \tag{C.29}$$

In the steady state, the flux of electrons must equal the flux of ions for quasineutrality requirements. This leads to define the ambipolar diffusion coefficient, D_a, in the Fick's law in absence of electric field:

$$\Gamma = -\frac{\mu_i D_e + \mu_e D_i}{\mu_i + \mu_e} \nabla n = -D_a \nabla n \tag{C.30}$$

where the sub-indexes i and e denote ions and electrons, respectively. The continuity equation (C.17) is then transformed into a diffusion equation, like equation C.29, that is valid for the both species, i.e, the ambipolar diffusion equation.

The macroscopic mobility constant, μ, shows an inverse relation with specie mass, m:

$$\mu = \frac{|q|}{m\upsilon_m} \tag{C.31}$$

where q is the electric charge and ν_m is the collision frequency. We note that, in the usual case of weakly ionised plasma, $\mu_e >> \mu_i$. The ambipolar diffusion coefficient results:

$$D_a = \frac{\mu_i D_e + \mu_e D_i}{\mu_i + \mu_e} \approx D_i + \frac{\mu_i}{\mu_e} D_e \tag{C.32}$$

The diffusivity is tied to the mobility through the Einstein relation:

$$D = \mu T \tag{C.33}$$

Hence, by replacing in equation C.32:

$$D_a \approx D_i \left(1 + \frac{T_e}{T_i}\right) \tag{C.34}$$

Therefore, the ambipolar diffusion is basically determined by the slow species (ions). Moreover, it is remarkable that the diffusivities of both electrons and ions (ambipolar diffusivity) greatly exceed in plasmas the diffusion rate of free ions, when the condition $T_e >> T_i$ is fulfilled.